Maturation of late Golgi cisternae into RabE^{RAB11} exocytic post-Golgi carriers visualized in vivo

Areti Pantazopoulou[a], Mario Pinar[a], Xin Xiang[b], and Miguel A. Peñalva[a]

[a]Department of Cellular and Molecular Biology, Centro de Investigaciones Biológicas, Consejo Superior de Investigaciones Científicas, Madrid 28040, Spain; [b]Department of Biochemistry and Molecular Biology, Uniformed Services University of the Health Sciences, Bethesda, MD 20814

ABSTRACT The mechanism(s) by which proteins traverse and exit the Golgi are incompletely understood. Using *Aspergillus nidulans* hyphae, we show that late Golgi cisternae undergo changes in composition to gradually lose Golgi identity while acquiring post-Golgi RabE^{RAB11} identity. This behavior of late Golgi cisternae is consistent with the cisternal maturation model. Post-Golgi RabE^{RAB11} carriers travel to, and accumulate at, the apex, indicating that fusion is rate limiting for exocytosis. These carriers, which are loaded with kinesin, dynein, and MyoE^{MYO5}, move on a microtubule-based bidirectional conveyor belt relaying them to actin, which ultimately focuses exocytosis at the apex. Dynein drags RabE^{RAB11} carriers away if engagement of MyoE^{MYO5} to actin cables fails. Microtubules seemingly cooperating with F-actin capture can sustain secretion if MyoE^{MYO5} is absent. Thus, filamentous fungal secretion involving post-Golgi carriers is remarkably similar, mechanistically, to the transport of melanosomes in melanocyte dendrites, even though melanosome biogenesis involves lysosomes rather than Golgi.

INTRODUCTION

A fascinating problem of cell biology is how lipids and proteins traverse the Golgi and are subsequently sorted into carriers bound to the plasma membrane and endosomes (Patterson *et al.*, 2008; Glick and Nakano, 2009; Glick and Luini, 2011). One model explaining this transit is the cisternal maturation model. It implies that Golgi cisternae are transient entities that form de novo from endoplasmic reticulum (ER)–derived traffic and undergo changes in lipid and protein content until reaching a compositional stage in which *trans*-most cisternae enriched in cargo break up into post-Golgi carriers (Glick and Nakano, 2009). A key observation was that Golgi cisternae of *Saccharomyces cerevisiae* are not stacked, such that early and late cisternae labeled with appropriate fluorescent protein markers are resolvable by light microscopy (Wooding and Pelham,

1998; for fungal cisternae we use the terms "early" and "late" instead of *cis* and *trans*, as the Golgi network lacks *cis*-to-*trans* spatial organization). Intra-Golgi maturation has been directly visualized in *S. cerevisiae* (Losev *et al.*, 2006; Matsuura-Tokita *et al.*, 2006). More recently, the exit from the late Golgi of sequentially assembled adaptor-specific populations of clathrin-coated vesicles destined to endosomes has also been visualized directly (Daboussi *et al.*, 2012). However, the transition of late Golgi cisternae to post-Golgi exocytic carriers has not.

The hyphal fungus *Aspergillus nidulans* is well suited to investigate exocytic traffic because early and late Golgi cisternae are also spatially resolvable by optical microscopy (Pantazopoulou and Peñalva, 2011) and secretion is polarized toward the growing tip (Taheri-Talesh *et al.*, 2008; Peñalva *et al.*, 2012; Pinar *et al.*, 2013a). Another advantage of *A. nidulans* hyphal tip cells is that although late Golgi cisternae are strongly polarized, they are excluded from the tip region, leaving a few micrometers between them and the apex (the target of exocytic carriers; Pantazopoulou and Peñalva, 2009). The presence of this gap facilitates the filming of post-Golgi events and implies that exocytic traffic between late Golgi cisternae and the apex requires long-distance transport.

Genetic screens using *S. cerevisiae* delineated the picture of the exocytic pathway in yeast and every other eukaryotic cell (Novick *et al.*, 1980; Bonifacino and Glick, 2004). Lipids and GTPases of the RAB family govern intracellular traffic (Behnia and Munro, 2005;

Barr, 2013). Work in *S. cerevisiae* strongly implicated the functionally overlapping paralogues and RAB11 family members Ypt31/Ypt32 in Golgi exit and transport between the Golgi and the sites of exocytosis (Jedd *et al.*, 1997; Morozova *et al.*, 2006; Lipatova *et al.*, 2008). Ypt31 is a key element of a "RAB cascade," a regulatory switch by which one RAB, Ypt31, directs the recruitment to membranes of the downstream-acting RAB, Sec4. Sec4 would take over Ypt31 regulatory functions to mediate vesicle tethering and fusion with the plasma membrane (Ortiz *et al.*, 2002). Similar RAB cascades would operate within the fungal Golgi (Rivera-Molina and Novick, 2009) and endosomal systems (Peplowska *et al.*, 2007; Nordmann *et al.*, 2010; Abenza *et al.*, 2012).

In addition to Golgi exit, exocytic RABs regulate transport of post-Golgi carriers to the plasma membrane. In yeast this step is powered by the type V myosin Myo2. Recruitment of Myo2 to exocytic carriers involves coincidence detection of either Ypt31 or Sec4 (which bind directly to the same region in the Myo2 cargo-binding domain) and of the lipid phosphatidylinositol 4-phosphate (PtdIns4P), with involvement of the exocyst component Sec15 (Lipatova *et al.*, 2008; Mizuno-Yamasaki *et al.*, 2010; Jin *et al.*, 2011; Santiago-Tirado *et al.*, 2011). At which point of transport Sec4 replaces Ypt31 and why two, instead of one, RABs are involved, despite the fact that Ypt31 and Sec4 share a number of effectors, including the exocyst, is not fully understood.

In yeast the reason possibly reflects the fact that Ypt31 acts near Golgi exit, whereas Sec4 and its prototypic effector, the exocyst, are involved in vesicle fusion, that is, near the end of the pathway, with the "RAB cascade" ensuring order and directionality. Unlike mammalian and filamentous fungal cells *S. cerevisiae* exocytosis relies solely on actin-based transport, which might be reflected in the major importance of Sec4, given that Sec4 coordinates tethering and soluble *N*-ethylmaleimide–sensitive factor attachment protein receptor (SNARE) regulation with the release of vesicles from Myo2 (Donovan and Bretscher, 2012).

In fungal hyphae and higher eukaryotic cells, microtubules (MTs) and F-actin cooperate in intracellular transport. In *Ustilago-maydis* yeasts, kinesin-1 and myosin-5 act in parallel to deliver exocytic carriers to the plasma membrane (Schuster *et al.*, 2012). In *A. nidulans*, current models depict MTs as mediating long-distance exocytic transport to the tip, whereas F-actin would mediate transport to the apex within the tip-proximal region (Taheri-Talesh *et al.*, 2008, 2012; Abenza *et al.*, 2009; Zhang *et al.*, 2011). Deletion of the single *A. nidulans* type V myosin gene, *myoE*, slows but does not prevent exocytosis, indicating that MT-dependent mechanisms must be operating (Taheri-Talesh *et al.*, 2012). Indeed, cells in which MyoE is down-regulated cannot even establish polarity if MTs are depolymerized, and MyoE down-regulation becomes lethal when combined with *kinAΔ*, removing the sole *A. nidulans* kinesin-1 (Requena *et al.*, 2001; Zhang *et al.*, 2011). However, the absence of robust exocytic markers has thus far precluded the direct confirmation of this cooperation.

Here we show how virtually every late Golgi cisterna matures into a post-Golgi structure by acquisition of the sole Ypt31 *A. nidulans* orthologue RabE[RAB11]. These post-Golgi membranes engage motors and undergo movement to the apex, where they accumulate, awaiting fusion. MTs and actin cables cooperate in this transport, although MTs are sufficient if MyoE is absent. Actin depolymerization displaces exocytic carriers containing MyoE, dynein, and at least one kinesin to a MT-based conveyor belt that constantly refills the tip umbrella of actin cables with post-Golgi carriers.

RESULTS

The *A. nidulans* exocytic Rabs, RabE[RAB11] and RabD[RAB8]

Exocytosis is required to maintain the integrity of the fungal cell wall. In *S. cerevisiae*, exocytosis is regulated by RAB cascade involving the pair of Ypt31/Ypt32 paralogues and Sec4 (Ortiz *et al.*, 2002). *A. nidulans* has single orthologues of Ypt31/Ypt32/RAB11 and Sec4, denoted RabE and RabD, respectively. RabE[RAB11] is essential (Figure 1A and Supplemental Figure S1, A–C). RabD[RAB8], although not essential (Supplemental Figure S1, D–F), is important for growth, as shown by the markedly reduced colony size resulting from *rabDΔ* (Figure 1B; the *rabDΔ* colony phenotype segregates as a single Mendelian character). Here we use RabE[RAB11] to study the biogenesis and delivery of post-Golgi exocytic carriers. The characterization of RabD[RAB8] will be reported elsewhere.

To investigate the subcellular localization of RabE[RAB11], for a majority of experiments we used a construct driving expression of green fluorescent protein (GFP)–RabE under the control of its own promoter, integrated at the *rabE* locus through a single crossover, which resulted in a tandem duplication of *rabE* in which only one of the copies is tagged with GFP (strain MAD4120 in Supplemental Table S1; complete description in Supplemental Figure S2 and *Materials and Methods*). We chose this genetic arrangement involving a "backup copy" of untagged RabE[RAB11] to avoid hypomorphic effects due to impaired function and/or reduced steady-state levels potentially resulting from endogenous GFP tagging (*rabE* is stringently essential); indeed, Western blot analyses with anti-RabE[RAB11] polyclonal antiserum showed that the steady-state levels of GFP-RabE in MAD4120 were 3.5 times lower than those of untagged RabE[RAB11], showing that the GFP-tagging procedure impairs protein expression/stability (Supplemental Figure S2). In parallel experiments, we showed by gene replacement that endogenous tagging of RabE[RAB11] with GFP (without a backup untagged copy) resulted in a similar 3.5-times reduction in steady-state levels (Supplemental Figure S2). However, even though this gene-replaced allele impairs growth, it rescues lethality and supports vegetative growth very substantially (Supplemental Figure S2). We also confirmed that the RabE[RAB11] subcellular distribution visualized by endogenous tagging was comparable to that seen with the tandem duplication allele (Supplemental Figure S2). Data detailed later showed that GFP-RabE[RAB11] recruitment to membranes depends on the GTP switch and on normal Golgi function. For some localization experiments, including all of those requiring mCherry-RabE[RAB11], we used the alcohol dehydrogenase promoter (*alcA[P]*), which allows manipulation of fusion protein levels by the carbon source of the medium (these *alcA[P]* strains also contain the resident untagged *rabE* copy). Supplemental Figure S2 includes comparative Western blot analyses showing the different expression levels of RabE[RAB11] attainable with the *alcA[P]* by manipulating the carbon source.

RabE[RAB11] is present in three types of structures (Figure 1C and Supplemental Movie S1): 1) punctate cytosolic structures, polarized toward the tip; 2) rapidly moving cytosolic structures; and 3) a conspicuous accumulation of membranes at the apex, subjacent to the plasma membrane. RabE[RAB11] localization to all these structures is nucleotide switch dependent because Ser23Asn substitution in RabE[RAB11] resulted in marked relocalization to the cytosol, with faint, diffuse fluorescence in endomembranes possibly representing the ER (Figure 1D). (The ER seems to be the "default" localization of the proportion of Rab-GDP that constantly sounds membranes; Cabrera and Ungermann, 2013.) Later we demonstrate that RabE[RAB11] cytosolic structures correspond to post-Golgi membrane domains forming by maturation of late Golgi cisternae (LGC), moving structures represent exocytic RabE[RAB11] carriers deriving from these domains
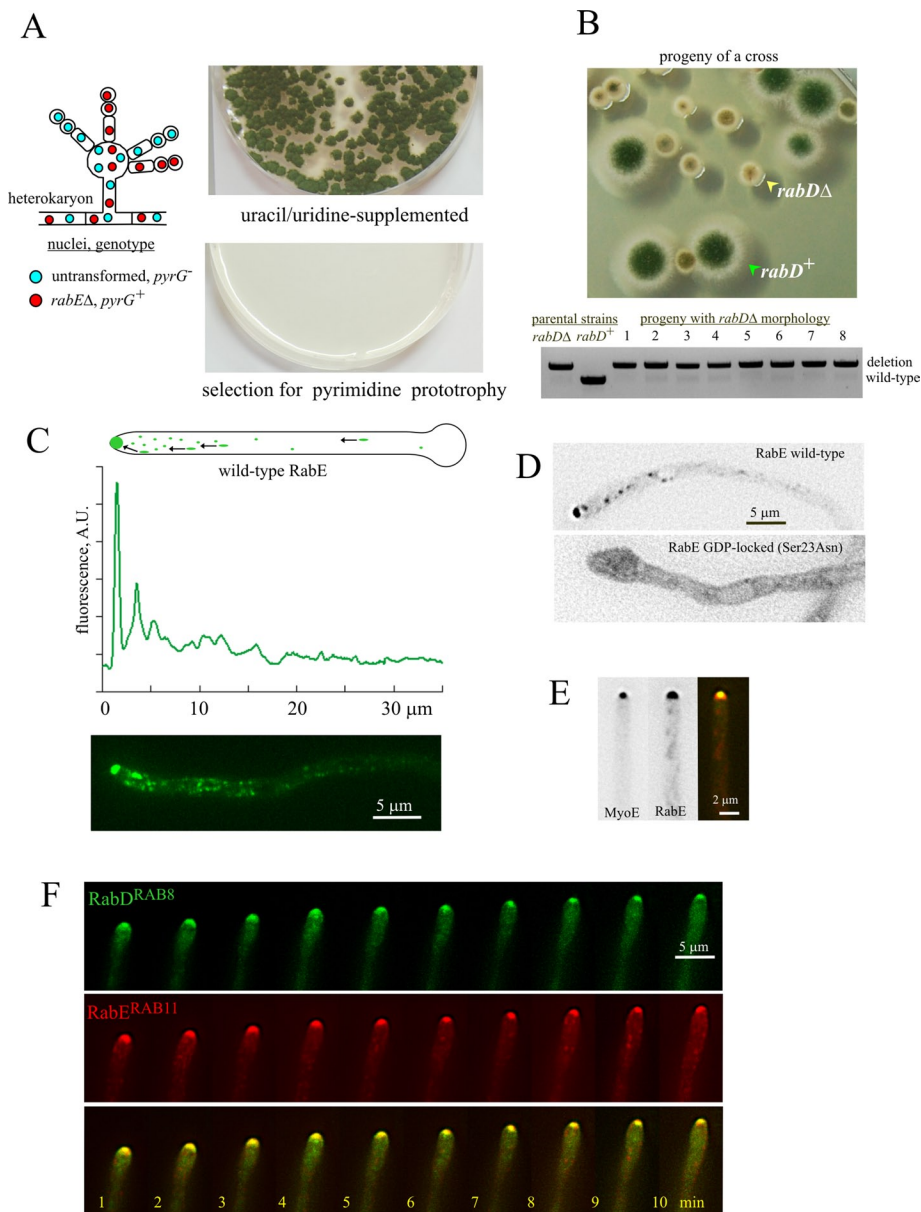
FIGURE 1: The exocytic *A. nidulans* RABs, RabE[RAB11] and RabD[RAB8]. (A) Heterokaryon rescue test (Osmani *et al.*, 2006) demonstrating that *rabE* is essential. (B) Progeny of a cross between *rabD+* and *rabDΔ* strains showing the *rabDΔ* growth phenotype, and diagnostic PCR establishing that eight random progeny with this growth phenotype contained the deletion allele. (C) Distribution of GFP-RabE. Expression was driven by the *rabE[P]* (strain MAD4120; Supplemental Table S1). The top linescan shows its marked polarization. (D) GDP-locking Sec23Asn substitution delocalizes RabE[RAB11] to a cytosolic haze and to a faintly labeled network of endomembranes. Wild-type and mutant GFP-RabE[RAB11] (strains MAD4072 and MAD4271) were expressed under the control of the *alcA[P]*, which was induced for 3 h after shifting cells to medium containing ethanol. Despite the fact that this regime results in GFP-RabE[RAB11] overexpression (see text and Supplemental Figure S2), the subcellular distribution of the wild-type fusion protein is indistinguishable from that attained with the natural *rabE* promoter. Images are middle planes of Z-stacks that have been contrasted with the "unsharp mask" filter of MetaMorph to maximize detection of endomembranes in the mutant. (E) MyoE-GFP colocalizes with mCherry-RabE at the SPK. Images of strain MAD4403, in which MyoE was endogenously tagged with GFP and mCherry-RabE[RAB11] expression was driven by the *alcA[P]* promoter. Cells were cultured on fructose to obtain similar levels of fluorescence, which permitted simultaneous GFP and mCherry channel recording using a Dual View. Note that the localization patterns of mCherry-RabE[RAB11] and GFP-RabE[RAB11] are indistinguishable (see *Materials and Methods* and Supplemental Figure S2). (F) GFP-RabD and mCherry-RabE colocalize at the SPK in a growing hypha. This time series was obtained with strain MAD4156, in which both GFP-RabD[RAB8] and mCherry-RabE[RAB11] were expressed from single-copy *alcA[P]*-driven constructs targeted to the *pyroA* and *argB* loci, respectively.

and captured during their journey toward the site of delivery, and the apical dome accumulation reflects a dense concentration of these carriers once they have been transported to the apex but have not yet fused with the plasma membrane. This accumulation corresponds to the Spitzenkörper (SPK), a fungal-specific structure that in electron microscope images consists of vesicles intermingled with a mesh of actin microfilaments (Harris *et al.*, 2005; Hohmann-Marriott *et al.*, 2006). RabE[RAB11] colocalizes at this structure with both the myosin-5 MyoE and RabD[RAB8] (Figure 1, E and F; for MyoE, see Supplemental Movie S2), which is consistent with the role attributed to Sec4/RAB8 proteins in the fusion of exocytic carriers with the plasma membrane, acting downstream of Ypt31/RAB11.

Maturation of late Golgi cisternae into exocytic post-Golgi carriers

According to the cisternal maturation model, newly formed Golgi cisternae undergo changes in protein/lipid composition until reaching a stage at which they become competent for tearing off into post-Golgi carriers. Maturation of early into late Golgi cisternae has been observed in vivo in *S. cerevisiae* (Losev *et al.*, 2006; Matsuura-Tokita *et al.*, 2006). More recently, progression of LGC into Gga- and AP-1–containing clathrin-coated carriers destined to the endosomes has been thoroughly documented (Daboussi *et al.*, 2012). In contrast, the transition of LGC into post-Golgi carriers has not been visualized in vivo. To this end, we used monomeric red fluorescent protein (mRFP)–PH[OSBP] as specific reporter of the late Golgi (Pantazopoulou and Peñalva, 2009, 2011; Pinar *et al.*, 2013a). PH[OSBP] is a peripheral protein recruited to membranes through coincidence detection of PtdIns4P and Arf1 (Levine and Munro, 2002). We previously showed that PH[OSBP] colocalizes with the *A. nidulans* Sec7 orthologue, HypB[Sec7] (Pantazopoulou and Peñalva, 2009). Cytosolic RabE[RAB11] structures showed little colocalization with PH[OSBP] puncta corresponding to LGC (Figure 2A), which is consistent with the former representing post-Golgi. Next we cofilmed RabE[RAB11] and PH[OSBP], acquiring Z-stacks of the green and red channels simultaneously every 3–4 s for several minutes (Supplemental Movie S3), which were analyzed with kymographs. In these plots, LGC appeared as tilted vertical lines that gradually lose intensity until they become undetectable (Figure 2B), indicating that LGC are transient structures that eventually dissipate, an observation consistent

with the cisternal maturation model (Matsuura-Tokita *et al.*, 2006). The RabE^{RAB11}-channel kymographs (Figure 2B), "capped" at the apexes by a prominent line corresponding to the SPK, suggested that cytosolic RabE^{RAB11} structures arise by recruitment of RabE^{RAB11} to dissipating LGC. As a result, PH^{OSBP} and RabE^{RAB11} overlapped, but only momentarily, because the RabE^{RAB11} signal associated with any given LGC increased with time as the PH^{OSBP} signal declined until becoming barely, if at all, detectable (89% of $n = 141$ mRFP-PH^{OSBP} LGC from six different hyphae were observed to mature to GFP-RabE^{RAB11}; Figure 2, B–D and F), and because coinciding with the peak of RabE^{RAB11} fluorescence, RabE^{RAB11} membranes underwent rapid movement toward the SPK, where they accumulated (Supplemental Movie S3; see later discussion). These departure events were seen as RabE^{RAB11} diagonal tracks "capping'" vertical LGC signals at their bottom ends (Figure 2, B–D). In summary, cytosolic RabE^{RAB11} structures originate from LGC that, we presume, undergo compositional changes to facilitate RabE^{RAB11} recruitment.

To increase time resolution, we acquired middle sections of growing hyphae every 100–250 ms (250–300 frames in total; Supplemental Movie S4), focusing kymographs on the transition between LGC and RabE^{RAB11} structures. These plots confirmed that the latter derive from the former (Figure 2, C and D). In addition, kymographs revealed that nascent RabE^{RAB11} structures could move toward the SPK following two different patterns: in some cases, the structure moved as whole entity (Figure 2C), whereas in other cases, once the RabE^{RAB11} structure was formed, it broke up into smaller "particles" (example in Figure 2D). Taken together, these experiments strongly suggest that Golgi exit involves a process by which mRFP-PH^{OSBP} membranes undergo changes in composition to mature into RabE^{RAB11} ones. Once RabE^{RAB11} reaches a certain level, these membranes undergo movement toward the site of exocytosis. These observations bear resemblance to the progressive PtdIns4P-dependent assembly of adaptor-specific clathrin coats during Golgi exit in the Golgi-to-endosome pathway (Daboussi *et al.*, 2012). By analyzing individual examples (Figure 2E, left) we determined that the average lifetime of LGCs was 120 s. Given that individual RabE^{RAB11} structures cannot be reliably tracked after they move toward the SPK, we determined their time of residence at the position of the "parental" LGC structure, before undergoing movement, which was 20 s (Figure 2E, right). Figure 2F provides a quantitative depiction of the transition between LGC and RabE^{RAB11} carriers for 10 different events.

Figure 3 (also see Supplemental Movie S3) shows a typical example in its cellular context, focusing on a LGC that can be easily tracked due to its characteristic ring shape (see magnified inset on the right). The biogenesis of post-Golgi carriers is preceded by the formation of an mRFP-PH^{OSBP} cisterna (boxed in red). After reaching a plateau, the mRFP-PH^{OSBP} content of the cisterna decreases, whereas RabE^{RAB11}, initially undetectable, becomes visible and progressively increases, such that at late steps of the "cycle" the structure is detectable mostly for its RabE^{RAB11} signal (boxed in green). Soon after RabE^{RAB11} becomes the "dominant" signal, the cisterna, initially spherical/ellipsoid, becomes stretched, as if submitted to tension, and moves toward the apex, accumulating under the apical dome plasma membrane.

To further confirm the maturation pathway of LGC into post-Golgi RabE^{RAB11} carriers, we used HypB^{Sec7} endogenously tagged with GFP (Pantazopoulou and Peñalva, 2009) to monitor LGC in combination with mCherry-RabE^{RAB11}. Owing to the weaker signal of HypB^{Sec7}, we expressed mCherry-RabE^{RAB11} under the control of the *alcA^P* promoter on fructose (which results in relatively low levels of expression of the protein; Supplemental Figure S2) in a strain

containing an untagged copy of *rabE*. Even though the weaker signals limited the time extension of four-dimensional image acquisition, movies derived from maximal-intensity projections of Z-stacks showed remarkably similar results to those described earlier (Supplemental Figure S3 and Supplemental Movie S5). Thus kymographs revealed that at the end of their lifespan, HypB^{Sec7} LGC are "capped" by mCherry-RabE^{RAB11} signals subsequently moving toward the apex. Analysis of the movies revealed that individual cisternae maturing into mCherry-RabE^{RAB11} could be tracked visually, and quantitation of the signals for individual cisternae in each channel revealed similar profiles to those seen with mRFP-PH^{OSBP} and GFP-RabE^{RAB11} (Supplemental Figure S3). Moreover, 96% of $n = 95$ HypB-^{Sec7}-GFP LGC (five different hyphae) were observed to mature to mCherry-RabE^{RAB11}. In summary, Golgi exit involves the gradual conversion of LGC into post-Golgi membranes by acquisition of RabE^{RAB11} and loss of Golgi identity. The resulting RabE^{RAB11} membranes undergo long-distance transport toward the apex, thus fulfilling the expected behavior for exocytic carriers.

The accumulation of RabE^{RAB11} carriers at the SPK depends on HypB^{Sec7}

The foregoing results suggest that the SPK accumulation of RabE^{RAB11} exocytic carriers reflects the balance between the biogenesis of these carriers from LGC, their transport to the apex, and their consumption by exocytosis. Thus impairment of Golgi exit should result in the reduction or dissipation of this structure. We tested this prediction by hindering the late Golgi activity of the key Golgi GTPase Arf1 with *hypB5*, a *ts* mutation in the gene encoding *A. nidulans* Sec7 (Yang *et al.*, 2008; Pinar *et al.*, 2013a), the late Golgi GEF of Arf1. In control experiments, we used the SynA synaptobrevin-like vesicle (v)-SNARE to label exocytic material. In the wild-type at both 28 and 37°C and in *hypB5* cells at 28°C, SynA, which is efficiently taken up from the plasma membrane by endocytosis, localizes to the apical crescent and to the SPK (Taheri-Talesh *et al.*, 2008; Pantazopoulou and Peñalva, 2011; Figure 4A). In contrast, in *hypB5* cells shifted to restrictive temperature (37°C), the SPK accumulation of SynA dissipated (as did the plasma membrane pool; Pinar *et al.*, 2013b; Figure 4A), as expected from impairment of Golgi exit. We next tested *hypB5* cells coexpressing PH^{OSBP} and RabE^{RAB11}. At 10–20 min after shifting *hypB5* cells to the restrictive temperature, the LGC marker PH^{OSBP} partially relocalized to the cytosol, consistent with impairment of late Golgi Arf1 activity (Figure 4B). Under these conditions, RabE^{RAB11} was completely delocalized from the SPK to internal structures (the SPK was undetectable in $n = 93$ *hypB5* hyphal tips photographed in two different experiments). These internal RabE^{RAB11} structures did not overlap with LGC remnants, suggesting that they have post-Golgi identity (Figure 4B). Neither SynA nor RabE^{RAB11} delocalization from the SPK reflected cell death because their normal distribution was restored when the temperature was shifted down subsequently (Figure 4, A and B). Thus late Golgi Arf1 GEF impairment delocalizes RabE^{RAB11} but does not prevent RabE^{RAB11} engagement with membranes.

In addition to their secretory roles, yeast Ypt31/Ypt32 regulate endosome-to-Golgi transport in a process involving their F-box effector Rcy1 (Chen *et al.*, 2005, 2011). Early endosomes of filamentous fungi are characteristically motile (Lenz *et al.*, 2006; Abenza *et al.*, 2009). Data to be described later established unambiguously that under normal circumstances, RabE^{RAB11} moving structures and RabA^{RAB5} early endosomes (EEs) are different populations. However, the acute perturbation of the Golgi by *hypB5* likely results in severe disruption of endosome-to-Golgi traffic. Thus we considered the possibility that the abnormal *hypB5*
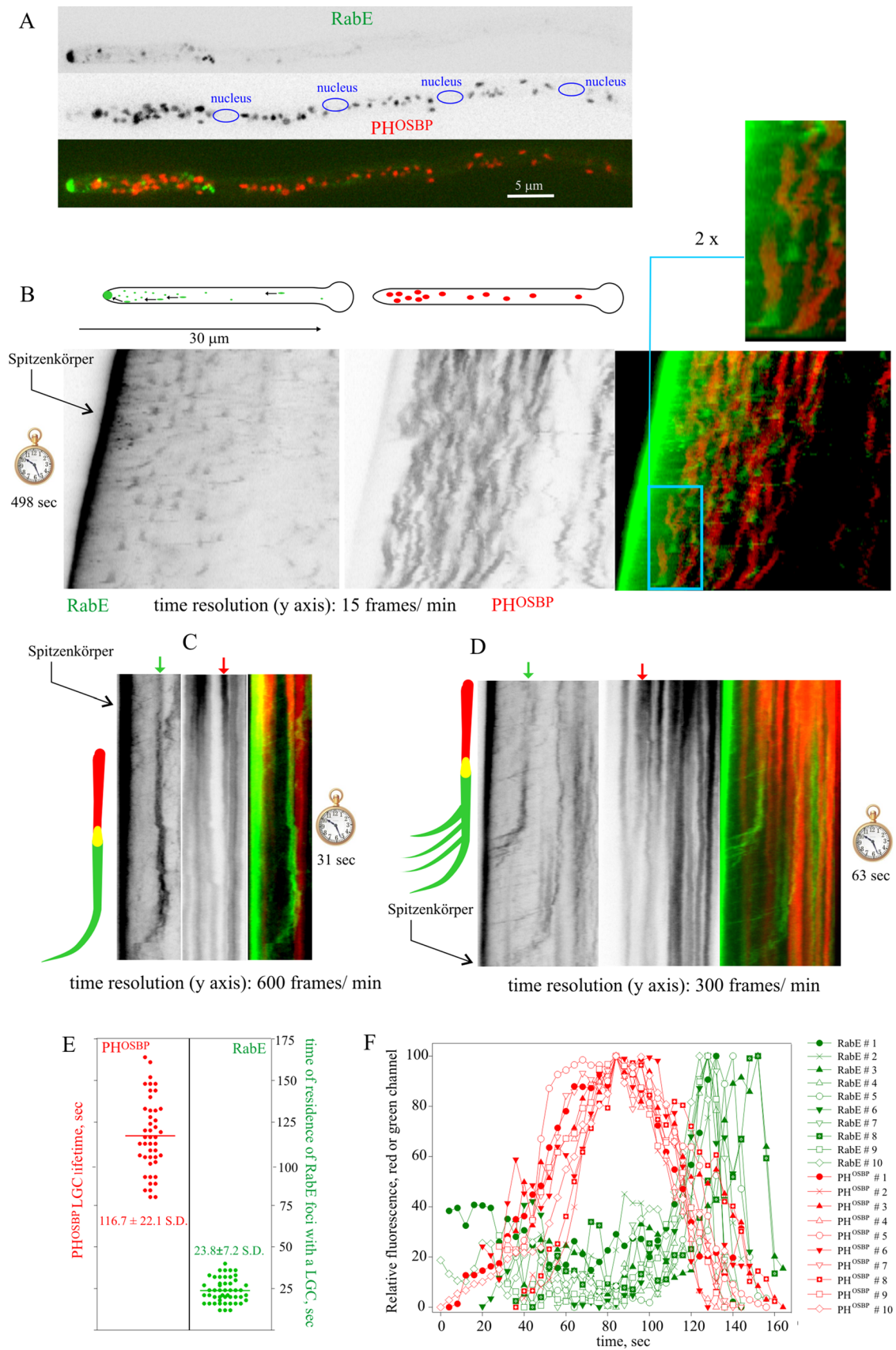
FIGURE 2: Maturation of LGC into post-Golgi carriers. Strain MAD4440. (A) GFP-RabE structures and mRFP-PH^{OSBP} LGC do not colocalize. (B) Kymographs of GFP-RabE and mRFP-PH^{OSBP} channels derived from time series constructed with projections of Z-stacks acquired every 4 s. The blue inset in the merge image is shown at double magnification. (C, D) Kymographs of GFP-RabE and mRFP-PH^{OSBP} derived from middle-plane time series with the indicated time
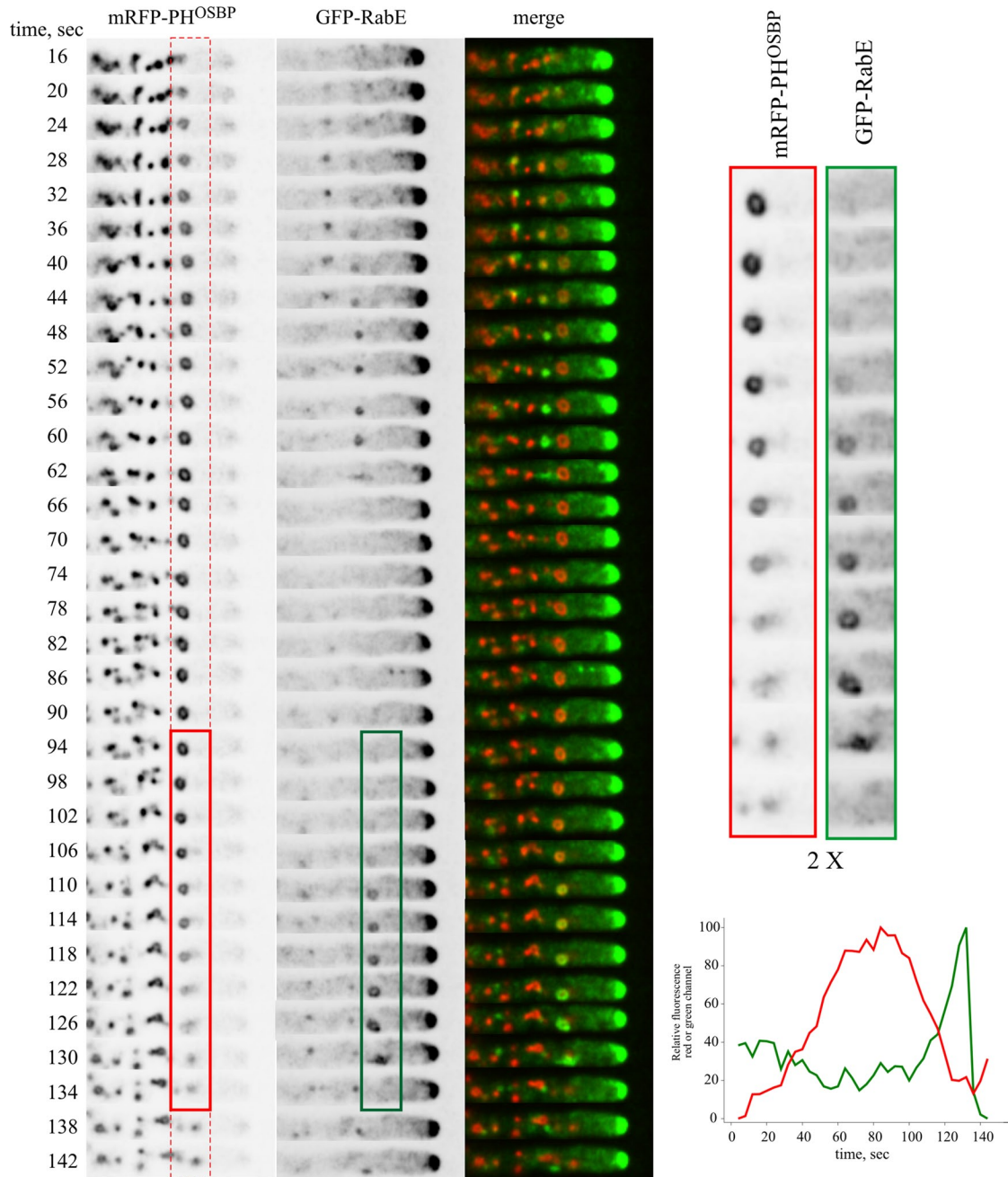
FIGURE 3: Maturation of LGC into post-Golgi carriers: an example in its cellular context. Boxed in red and green is an mRFP-PH[OSBP] cisterna that matures into a GFP-RabE post-Golgi structure that undergoes movement at the 130-s time point. The relative fluorescence in the red and green channels is plotted against time. Relevant time points of the two channels corresponding to this structure are magnified on the right to illustrate the match in shape between mRFP-PH[OSBP] and GFP-RabE. Frames are from Supplemental Movie S3 (strain MAD4440).

RabE[RAB11]–containing structures might represent stranded membranes with some degree of endosomal identity. We tested this possibility with a *hypB5* strain coexpressing GFP-RabE[RAB11] and mCherry-tagged early endosomal RabA[RAB5]. RabE[RAB11] and RabA[RAB5] partially overlapped in this abnormal compartment (Supplemental Figure S4), which might be consistent with RabE[RAB11] playing a role in this recycling pathway. In any case, experiments with *hypB5* demonstrated that the maintenance of the steady-state pool of RabE[RAB11] membranes at the SPK necessitates late Golgi Arf1 activity.

resolution. Schemes illustrating the two modes of movement of post-Golgi carriers to the apex also depict an interpretation of the changes undergone by the arrowed cisternae. (E) Left, average lifetimes of mRFP-PH[OSBP] LGC. Right, time of residence of GFP-RabE foci associated with a maturing LGC before it undergoes movement toward the SPK. (F) Quantitation of mRFP-PH[OSBP] and GFP-RabE fluorescence data for *n* = 10 cisternae over ~160 s. The sharp decay of GFP-RabE fluorescence corresponds to the time at which the corresponding focus undergoes movement toward the apex.
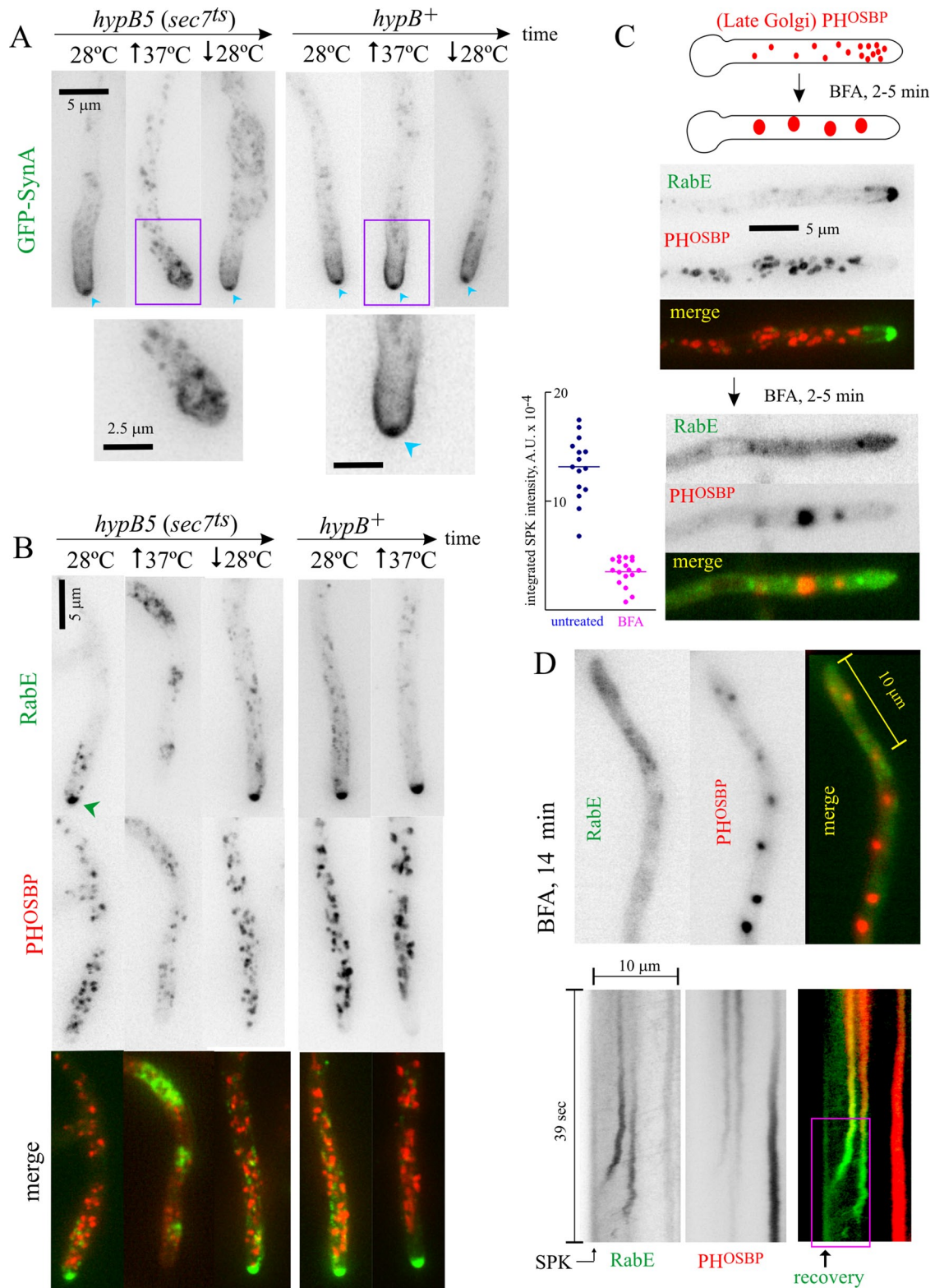
FIGURE 4: Membranes containing RabE^{RAB11} have post-Golgi identity. (A) Temperature shift experiment comparing *hypB5^{ts}* (*sec7^{ts}*) and *hypB$^+$* strains (MAD3323 and MAD3320, respectively) expressing GFP-SynA to label the accumulation of exocytic membranes at the position of the SPK (indicated when present with blue arrowheads). Upward- and downward-pointing arrows indicate temperature shift up and down, respectively. The regions indicated by the violet boxes are displayed at the bottom at double magnification. (B) *hypB5^{ts}* (*sec7^{ts}*) and *hypB$^+$* strains (MAD3632 and MAD3167, respectively, expressing mRFP-PH^{OSBP} and GFP-RabE^{RAB11}, the latter under the control of the *alcA^p* on ethanol). In a control experiment with strain MAD5082 we confirmed that the same abnormal compartment was formed when GFP-RabE^{RAB11} expression was driven by the *rabE* promoter in a strain that did not express mRFP-PH^{OSBP}. See also Supplemental Figure S4. (C) Top, aggregation of Golgi cisternae by BFA treatment. Bottom, mRFP-PH^{OSBP} LGC

The accumulation of post-Golgi RabE^RAB11 carriers at the SPK is largely reduced by brefeldin A

If Golgi traffic is abrogated, the biogenesis of post-Golgi compartments should be abolished immediately. We used brefeldin A (BFA) to interfere with Golgi traffic. Unlike *hypB5*, BFA impairs both the early and late Golgi activity of Arf1. In *A. nidulans* this leads to disorganization of the Golgi network, resulting in almost immediate (within 5–10 min) coalescence of cisternae into large aggregates (Pantazopoulou and Peñalva, 2009, 2011; Figure 4C). Instead of behaving like Golgi cisternae, cytosolic RabE^RAB11 structures, including SPK accumulation, which was markedly reduced (Figure 4, C, and D, kymograph; note that the effect of BFA is incomplete and transient; see later discussion), rapidly delocalized to a cytosolic haze. These data imply that dysfunction of the Golgi network impairs the biogenesis of RabE^RAB11 carriers. Because Golgi-resident RabO^RAB1 and RabC^RAB6, as well as Golgi cisternae labeled with resident SNAREs, rapidly aggregate with BFA (Pantazopoulou and Peñalva, 2011; Pinar et al., 2013a), we conclude that RabE^RAB11 membranes do not belong to the "Arf1 domain" (i.e., they lack Golgi identity), which strongly supports their post-Golgi nature.

After the initial ~15-min period in the presence of BFA, the Golgi starts to recover spontaneously, albeit slowly (Pantazopoulou and Peñalva, 2009). Thus, at 15 min and later, cells that had been clearly affected by BFA (impaired exocytosis leads to tip swelling; Pinar et al., 2013a,b) displayed a gradual recovery of RabE^RAB11 at their apexes, with both the prominence of these "SPK primordia" and the number of hyphal tip cells showing them clearly increasing with time. This indicated that gradual recovery of the Golgi was paralleled by gradual recovery of the SPK. During the recovery phase, we were able to recognize isolated examples of maturation in which we tracked more easily the fate of post-Golgi RabE^RAB11 structures without the interference of the strong SPK signal. The kymograph in Figure 4D depicts a hyphal tip filmed during this phase. Two PH^OSBP puncta mature into RabE^RAB11-positive membranes that undergo movement toward the apex. Their arrival at the environs of the plasma membrane is detectable by the increase in GFP-RabE^RAB11 fluorescence. The correlation between recovery of the apical accumulation of RabE^RAB11 and reassumption of Golgi function that occurs as cells recover spontaneously from BFA established beyond doubt that building the SPK requires Golgi exit.

The SPK cluster of RabE^RAB11 is rapidly replenished by carriers

Fluorescence recovery after photobleaching (FRAP) experiments established that the SPK is indeed rapidly replenished with RabE^RAB11 (Figure 5, A and B; $t_{1/2} \approx 10$ s). We attributed this rapid FRAP recovery to the strikingly fast and intense acropetal (i.e., toward the apex) traffic of RabE^RAB11 carriers bombarding the apex. This traffic was recorded by wide-field microscopy, streaming middle-plane sequences of 200–900 images acquired at 5–10 frames/s to the computer RAM (Supplemental Movie S1). Carrier trajectories were tracked with kymographs (Figure 5C). In the ~3-min/900-frame sequence used for this kymograph, 47 such carriers actually hit the SPK, but this is an underestimation, as a proportion of carriers was inevitably lost by single-plane sequences taken with low exposure times to minimize photodamage. In $n = 9$ tips, 73% of RabE^RAB11

carriers moved toward the SPK, whereas 24% moved basipetally (Figure 5D).

Acropetal trajectories were in two classes. Carriers with the strongest signal and most apical tracks moved intermittently and generally more slowly. Their trajectories reflect the movement en masse of large RabE^RAB11 structures to the SPK (Figure 5E, 1–5). The smallest carriers/weakest signals represented the majority of trajectories and involved structures moving several micrometers at uniform speeds (Figure 5E, orange box). They often moved acropetally for some distance before reversing direction (Figure 5C, box) or stopping in the tip at positions generally coinciding with larger RabE^RAB11 puncta (Figure 5E, box). This suggested that many such "small carriers" might not travel completely to the plasma membrane, contrasting with large RabE^RAB11 carrier movements, which would appear to represent the membrane-proximal exocytic transport step.

Post-Golgi carriers travel toward and away from the apex on MTs

Evidence that many RabE^RAB11 carriers move acropetally on MTs is compelling. Benomyl markedly reduced the accumulation of carriers at the SPK (Figure 5F) and virtually abolished movement (Supplemental Figure S5). However, as we were concerned that benomyl might affect F-actin indirectly, we cofilmed GFP-RabE^RAB11 and GFP–α-tubulin (TubA)–labeled MTs. These movies, in which RabE^RAB11 carriers can be distinguished unambiguously from long, stiff MTs, established that the former move associated with the latter (Supplemental Movies S6 and S7).

RabE^RAB11 carriers were able to move basipetally (Figure 5G). Because the plus ends of tip MTs are oriented toward the apex (Konzack et al., 2005), these basipetal trajectories must reflect attachment to MTs undergoing catastrophe or dynein-dependent transport. Coimaging of TubA and RabE^RAB11 captured basipetal movements associated with MTs, strongly indicating that they are dynein mediated (Supplemental Movie S7). Physiologically, dynein engagement provides the secretory system with the capacity to drag post-Golgi membranes away from the tip region.

The average speed of RabE^RAB11 carriers (2.67 ± 0.04 SEM μm/s; $n = 392$) and their changes in direction resemble those of EEs moving on MTs (Lenz et al., 2006; Abenza et al., 2009; Schuster et al., 2011). We hypothesized that there might be a population of membranous carriers having both secretory and endocytic identity organized in mosaics of two different RAB domains. However, cofilming EEs labeled with RabA^RAB5 and exocytic carriers labeled with RabE^RAB11 simultaneously showed that EEs and RabE^RAB11 moving structures represent distinct entities (Supplemental Figure S6). In a second set of experiments, we labeled endosomes with FYVE_2-GFP. This probe consists of a tandem duplication of the Vps27 FYVE domain fused to GFP (Abenza et al., 2010). FYVE_2-GFP efficiently binds phosphatidylinositol 3-phosphate, which is present on the membranes of endosomes but absent from exocytic compartments. Cofilming of mCherry-RabE^RAB11 carriers with FYVE_2-GFP endosomes revealed that the two populations of moving structures are clearly different: the number of RabE^RAB11 "movements" clearly outnumbers that of FYVE_2-GFP endosomes, and the corresponding kymograph traces hardly, if at all, overlapped (Supplemental Figure S7).

aggregate with BFA, whereas GFP-RabE membranes delocalize to a haze (strain MAD4440). Left, SPK accumulation of RabE^RAB11 carriers is largely dissipated by BFA. The two sets of data are significantly different ($p < 0.0001$). (D) Two tip-proximal cisternae recovering from BFA treatment. The line depicts the region of interest used to plot the bottom kymograph. The two LGCs progressively acquire RabE^RAB11 and move toward the SPK, where their arrival results in a detectable increase in GFP fluorescence.
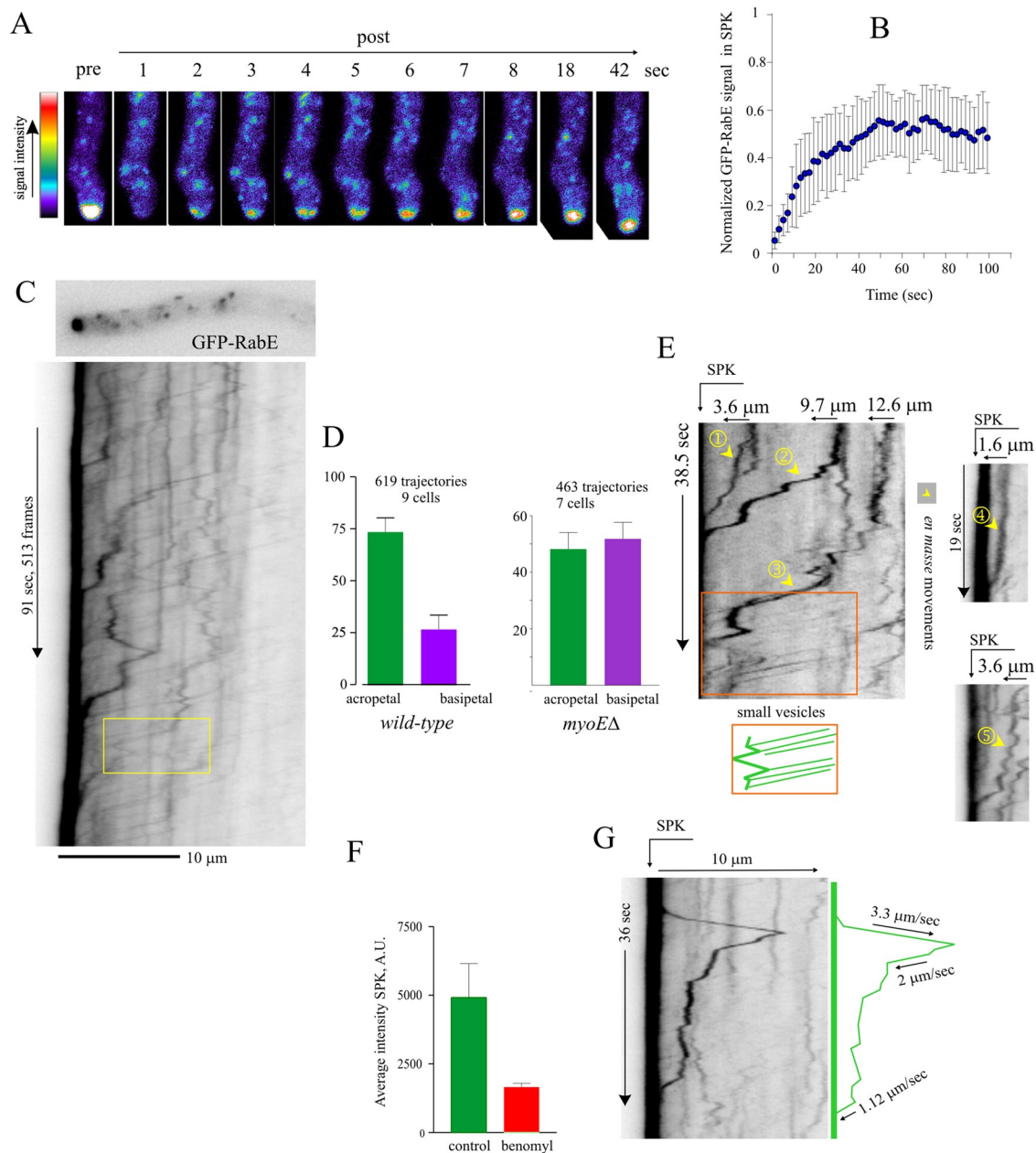
FIGURE 5: Intense bombardment of the apical region by exocytic RabE[RAB11] traffic. (A) Still-frame micrographs showing fast FRAP recovery of the SPK GFP-RabE signal. (B) Normalized GFP-RabE signal in the SPK after bleach event. Error bars are SD of n = 6 cells. (C) Kymograph traced across the axis of the depicted hyphal tip. Yellow box indicates an acropetally moving carrier that reverses direction. Derived from Supplemental Movie S1. (D) Percentage of acropetal and basipetal GFP-RabE trajectories in wild-type and *myoEΔ* cells. Error bars are SD. (E) Kymograph plots depicting five examples of large GFP-RabE carriers moving to the SPK and an area (boxed) depicting intense traffic of small carriers with uniform speeds. (F) Average intensity of the GFP-RabE SPK measured in sum projections of *Z*-stacks of images from cells treated or not with 10 µg/ml benomyl. (G) Kymograph depicting basipetal movement of a large GFP-RabE carrier. Experiments were carried out with strain MAD4120 and its *myoEΔ* derivative, MAD4409.

Actin-dependent mechanisms are crucial for the apical delivery of RabE[RAB11] carriers

F-actin cooperates with MTs to maintain tip growth (Torralba *et al.*, 1998; Sharpless and Harris, 2002; Virag *et al.*, 2007; Taheri-Talesh *et al.*, 2008, 2012; Zhang *et al.*, 2011). In current models the F-actin role involves a dense mesh of actin cables that radiates from the SPK (Pearson *et al.*, 2004; Taheri-Talesh *et al.*, 2008). These cables are flexible, resembling the strings of a mop. They can penetrate as

deeply as 25 µm into the hyphal cell (Taheri-Talesh *et al.*, 2012), such that polarized LGC (Pantazopoulou and Peñalva, 2009) fall within their reach.

F-actin depolymerization with latB arrested growth and rapidly delocalized RabE[RAB11] from the SPK (Figure 6A) without noticeably affecting MT organization (Supplemental Figure S5), showing that exocytosis requires F-actin. The fact that exocytosis can proceed to some extent without MTs (Figure 5F; Horio and Oakley, 2005) but

not without actin filaments indicates that actin and MTs cannot mediate redundant parallel transport pathways, suggesting instead that MTs are subordinated to actin.

The contention that F-actin acts downstream of MTs was strongly supported by the finding that latB displaced all RabE[RAB11] membranes, including those in the SPK, to a conspicuous population of rapidly moving structures showing bidirectional movement and average speed (3.15 ± 0.06 SEM µm/s; n = 231) consistent with MT motor powering (Figure 6A and Supplemental Movie S8). Coimaging of RabE[RAB11] and TubA-GFP in these latB-treated cells provided indisputable evidence that these structures move on MTs (Supplemental Movie S9). Indeed, when F-actin and MTs were depolymerized simultaneously, RabE[RAB11] membranes formed static aggregates that did not colocalize with PH[OSBP] (Supplemental Figure S8). Therefore, in the absence of F-actin, secretory carriers can arrive at the tip on MTs, but they are dragged out, presumably, by dynein. These findings indicate that MTs fuel the tip region with exocytic carriers, relaying them to an F-actin–dependent motor that mediates the last step in their transport to the SPK. MT transport works like a "conveyor belt" that shows up clearly if actin is depolymerized. This mechanism ensures that if the actin/MT "relay" is missed, RabE[RAB11]-containing membranes are dragged out away from the tip by dynein (see later discussion)

Myosin V focuses RabE[RAB11] carriers at the apex, but F-actin plays roles beyond providing tracks

The single *A. nidulans* class V myosin, MyoE, colocalizes with the v-SNARE SynA[Snc1] (Taheri-Talesh *et al.*, 2012) and RabE[RAB11] (Figure 1E) at the SPK, which is consistent with MyoE powering the actin-dependent step in exocytosis. *myoEΔ* markedly slows down, yet does not arrest, apical extension (Taheri-Talesh *et al.*, 2012), showing that the MyoE role, albeit important, is not essential. In agreement, in *myoEΔ* cells, RabE[RAB11] carriers moved toward the tip and arrived at the plasma membrane. However, they could not be "focused," spreading into an apical crescent instead of gathering at the apex (Figure 6B). Thus MyoE focuses RabE[RAB11] carriers at the apex via actin cables. Hardly any acropetal movements of the large RabE[RAB11] structures were seen in *myoEΔ* tips (Supplemental Movie S10), supporting the contention that these movements involve actomyosin.

RabE[RAB11] carriers must use MTs to arrive at the *myoEΔ* apical crescent. Within this crescent, the RabE[RAB11] signal appeared strongest in a ring immediately upstream from the apex (Figure 6B), as if this area, frequently contacted by MTs (Supplemental Figure S5), represented a preferred landing spot for carriers. Evidence that *myoEΔ* secretion is indeed MT dependent was compelling: movies captured carriers en route to the crescent, kymographs demonstrated that MT-like bidirectional transport was associated with cortical MTs (Figure 6C), and trajectories revealed by projecting time stacks onto a two-dimensional (2D) image clearly delineated MTs (Figure 6D).

myoEΔ markedly increased the number of basipetal movements in the tips (Figure 5D), showing that failure to engage MyoE increases the chance that RabE[RAB11] membranes will be dragged away from the tip by dynein. However, in contrast to actin depolymerization (Figure 6A), *myoEΔ* did not shift apical RabE[RAB11] material to the "MT conveyor belt," indicating that F-actin is able to "capture" RabE[RAB11] carriers even when myosin V is completely absent. *myoEΔ* tips showed a tip haze of RabE[RAB11] (Figure 6, B–E) that movies resolved as string-like structures dangling from the apex, whose resemblance to tropomyosin-labeled structures indicated that they are microfilaments decorated with RabE[RAB11] (Figure 6F and Supplemental Movie S11). Hence secretory carriers cannot move on cables without MyoE but are capable of binding them, explaining the inability of *myoEΔ* to shift all of these carriers to the MT-based conveyor belt. Indeed, latB dispersed the crescent-and-string–associated RabE[RAB11] material of *myoEΔ* tips to moving structures (Figure 6E). Benomyl also dispersed this crescent-and-string–associated material, indicating that MTs supply the RabE[RAB11] membranes captured by F-actin. However, the resulting cytosolic structures were, as expected, immotile (Figure 6E and Supplemental Movie S11). We conclude that in *myoEΔ* cells, exocytosis is fueled by MTs with collaboration of a F-actin–dependent capture mechanism (the "actin mop").

RabE[RAB11] carriers moving with the MT conveyor belt are loaded with MyoE

The behavior of RabE[RAB11] carriers displaced to the conveyor belt by latB implies that they are loaded with dynein and kinesin(s). The seamless relay between MTs and actin cables might be easier if RabE[RAB11] carriers were also loaded with MyoE. Under normal conditions, exocytic carriers labeled with MyoE-GFP can hardly be tracked by time-lapse imaging because in the steady state MyoE almost exclusively localizes to the SPK, resulting in faint signals elsewhere (Taheri-Talesh *et al.*, 2012). To overcome this obstacle, we depolymerized F-actin with latB before cofilming MyoE-GFP and mCherry-RabE[RAB11] with a beam splitter and maximized detection by drawing 2D maximal-intensity projections of the resulting "time stacks." In untreated cells, projections revealed, besides the SPK, very faint signals for MyoE and, as described earlier, MT tracks for RabE[RAB11] (Figure 7A). Latrunculin B shifted both MyoE-GFP and mCherry-RabE[RAB11] from the SPK to the population of bidirectionally moving structures. The 2D projections of MyoE and RabE[RAB11] trajectories in latB cells colocalized, clearly delineating MTs (Figure 7A). The resulting increase of MyoE-GFP signal in the moving population sufficed to detect MyoE trajectories with kymographs, which established that MyoE-GFP and mCherry-RabE[RAB11] actually colocalize on the same moving structures (Figure 7B). Therefore MyoE is a passenger of RabE[RAB11] carriers relocalizing to the "MT conveyor belt" after F-actin depolymerization. These carriers move in both acropetal and basipetal directions (Figure 7B), implying that they are loaded with one (or more) kinesins, dynein, and MyoE riding as passenger. Figure 8 shows a model (see *Discussion*) depicting how maturation of post-Golgi carriers is integrated with transport to the apex by a MT-based conveyor belt that concentrates carriers in the tip region before they are relayed to MyoE transport.

DISCUSSION

How traffic traverses and exits the Golgi is a fundamental problem. The finding that nonstacked fungal Golgi cisternae are resolvable by fluorescence microscopy (Wooding and Pelham, 1998) paved the way for studies revealing that cisternae are transient entities undergoing changes in protein content by which early components are substituted by late components over time (Losev *et al.*, 2006; Matsuura-Tokita *et al.*, 2006). These observations met key predictions of the cisternal maturation model (Glick and Luini, 2011). In this model, Golgi cisternae forming by coalescence of ER-derived vesicles become progressively enriched in cargo as they advance across a maturation pathway until they reach a stage in which membranes and cargo exit the Golgi as carriers destined to the plasma membrane or endosomes (Glick and Nakano, 2009). The transient nature of late Golgi cisternae has been experimentally observed (Losev *et al.*, 2006; Matsuura-Tokita *et al.*, 2006). Recently the PtdIns4P-coupled biogenesis of endosome-destined Gga2p- and AP-1-enriched carriers from LGC (representing another maturation
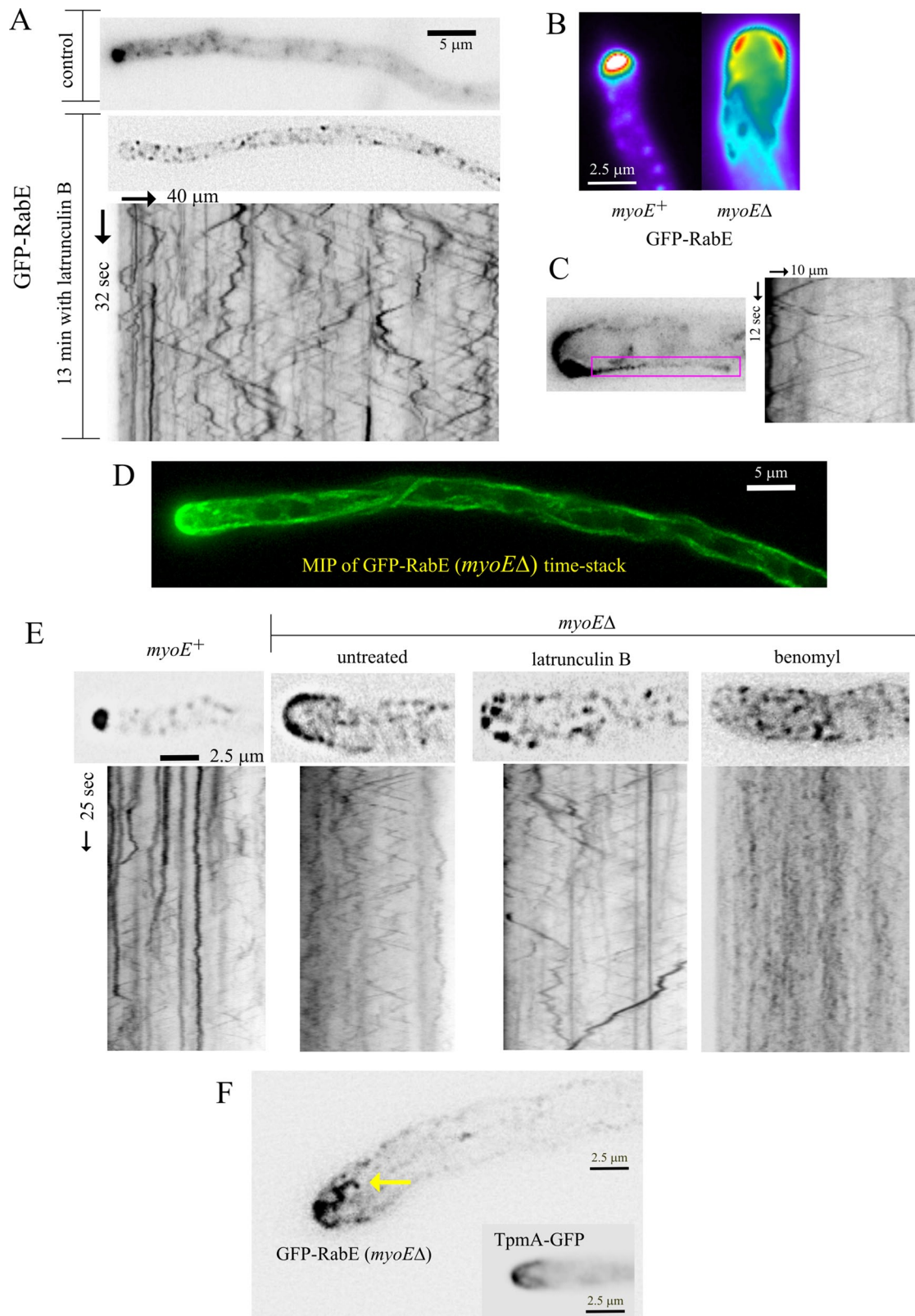
FIGURE 6: MyoE-dependent and -independent functions of F-actin. (A) Latrunculin B treatment delocalizes GFP-RabE–containing membranes at the SPK to the MT conveyor belt. Derived from Supplemental Movie S8. (B) An example of a *myoEΔ* tip in which the GFP-RabE crescent is thicker in a slightly subapical position. (C) Kymograph covering the position of a cortical MT, showing that it serves as track for RabE[RAB11] carriers moving in both directions and the uniform speeds characteristic of MT-dependent movements. (D) Maximal-intensity projection of a middle-plane time stack showing how moving GFP-RabE carriers delineate trajectories of MTs. (E) Micrographs from time stacks of images and the corresponding kymographs, showing effects of F-actin and MT depolymerization on the tip-and-apical crescent-associated GFP-RabE carriers. Both drugs delocalized these carriers from the tips of *myoEΔ* cells, but these
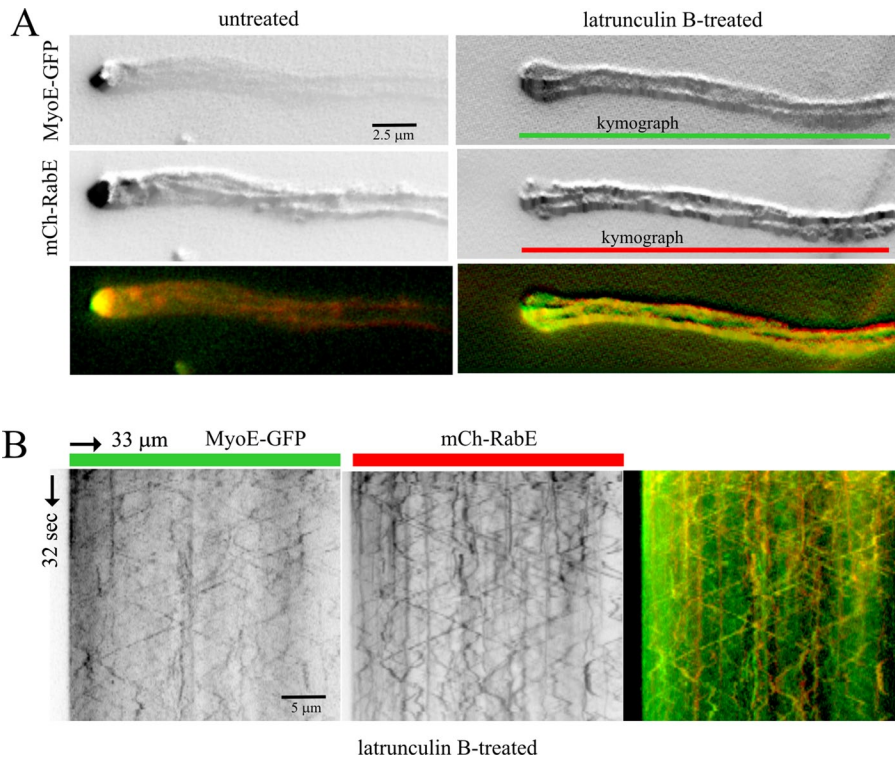
FIGURE 7: Latrunculin B displaces RabE^RAB11 carriers to MTs. (A) Maximal-intensity projection of middle-plane time stack showing trajectories of mCherry-RabE and MyoE-GFP. The finding that latB displaced carriers from the SPK to the MT conveyor belt allowed us to determine that the trajectories of MyoE and RabE colocalize, delineating MTs. (B) Kymograph of the latrunculin B–treated cell, showing how MyoE-GFP and mCherry-RabE colocalize on moving structures. These experiments were carried out with strain MAD4403 cultured on fructose, with MyoE-GFP being expressed from an endogenously tagged *myoE* allele (Taheri-Talesh *et al.*, 2012).

For example, yeast RAB11 homologue Ypt32 negates RAB6/Ypt6 activity by recruiting the Ypt6 GAP, Gyp6 (Suda *et al.*, 2013), and RAB1/Ypt1 activity by recruiting the "anti-current" Ypt1 GAP, Gyp1 (Rivera-Molina and Novick, 2009). The domain of action of Ypt1 (Sclafani *et al.*, 2010) and *A. nidulans* RabO^RAB1 (Pinar *et al.*, 2013a) possibly includes the late Golgi. Thus our data can be easily reconciled with previous work by expanding the regulatory function of RabO^RAB1 to the whole Golgi, leaving for RabE^RAB11 the role of mediating exocytic Golgi exit.

Golgi exit and subsequent transport of RabE^RAB11 carriers

The diffraction-limited spatial resolution of our time-resolved series precluded us from reaching a firm conclusion on whether the exit of carriers involves budding of one or more vesicles from the same LGC or transport to the SPK of the whole membrane content of the LGC. However, in some cases in which the maturing LGC appeared as an optically resolvable hollow circle, as in the example of Figure 3, the shape of the resulting RabE^RAB11 structure precisely matched that of the parental LGC, indicating that at least in these cases the whole cisterna is involved in the biogenesis of the post-Golgi carrier. The fact that observations were reproduced when we used endogenously tagged HypB^Sec7 instead of PH^OSBP as LGC marker indicates that a major portion of the parental LGC is involved in the biogenesis of the post-Golgi carrier, which would meet one important prediction that derives from the cisternal maturation model, namely that after maturation, Golgi cisternae dissipate (Matsuura-Tokita *et al.*, 2006). However, the persistence of a weak signal in the position of "parental" LGCs (as in the Figure 3 example) suggests that not all the membrane of any given LGC is incorporated en bloc into a RabE^RAB11 carrier. This is not unexpected, given that LGC, in addition to generating exocytic carriers, deliver membrane vesicles toward the endosomes (Daboussi *et al.*, 2012) and that some membrane could be contributed to another cisterna via intra-Golgi retrograde transport. Although this work describes the overall landscape of the dynamic transition between the Golgi and exocytic carriers in *A. nidulans*, future work involving a wider set of markers to define more precisely both the composition and the fate of LGC and exocytic carriers, as well as superresolution to try to resolve membrane subdomains within them, will be required to delineate more precisely the mechanisms by which LGC give rise to exocytic membranes.

Direct imaging established that exocytosis requires cooperation of MT and F-actin, in agreement with genetic data (Zhang *et al.*, 2011; Taheri-Talesh *et al.*, 2012). MyoE focuses RabE^RAB11 carriers at the main site of exocytosis, the apex (Taheri-Talesh *et al.*, 2008), via actin filaments, whereas MT transport bulldozes post-Golgi

process at the exit of the Golgi) has been thoroughly documented (Daboussi *et al.*, 2012). In contrast, the transition between LGC membranes and exocytic carriers had not been imaged in vivo.

Maturation of LGC into exocytic carriers with post-Golgi identity

A. nidulans LGC are separated from the site of exocytic carrier delivery by a few-micrometer gap, facilitating the filming of the Golgi–to–post-Golgi transition during exocytosis. We predicted that the key determinant of post-Golgi identity would be RabE^RAB11 because Ypt31 (yeast RAB11) activation is critical for Golgi exit (Jedd *et al.*, 1997; Morozova *et al.*, 2006) and Ypt31 contributes to recruitment of Myo2 (the only motor mediating yeast exocytosis) to post-Golgi carriers (Lipatova *et al.*, 2008; Jin *et al.*, 2011; Santiago-Tirado *et al.*, 2011). In rapidly growing hyphal tip cells, the lifespan of LGC, as determined with PH^OSBP, is ~2 min. At the end of this period, LGC gradually lose Golgi identity as RabE^RAB11 is progressively recruited until it nearly becomes their only detectable marker. The peak of RabE^RAB11 content coincides with the engagement of motors, resulting in rapid movement to the apex. The average time of residence of RabE^RAB11 in association with LGC that precedes transport is ~20 s. The sharp transition between late Golgi and post-Golgi identity might be consistent with RabE^RAB11 "negating" Golgi identity.

carriers moved only when MTs were present. (F) Isolated frame from a time stack (Supplemental Movie S11) showing microfilament-like material decorated with GFP-RabE carriers. A hyphal tip in which actin cables are decorated with GFP-tropomyosin is shown for comparison. Experiments were carried out with strain MAD4120 and its *myoEΔ* derivative, MAD4409. The TpmA-GFP inset corresponds to MAD1750.
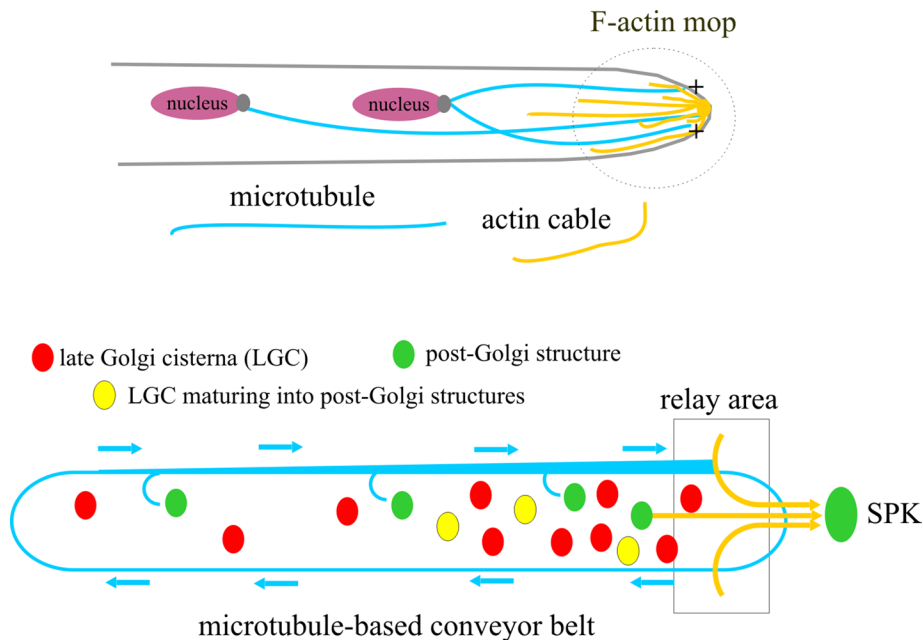
FIGURE 8: Model for the biogenesis and delivery to the apex of post-Golgi carriers. The biogenesis of RabE^RAB11 carriers from LGC is coupled to their long-distance transport to the apex by the concerted action of F-actin and a MT conveyor belt. The MT-based conveyor belt relays these carriers to the tip mop of microfilaments. See *Discussion* for details.

structures originating away from the tip toward the tip mesh of actin. Large RabE^RAB11 carriers show irregular speeds in kymographs and generally reach the apex. The movement of these large carriers possibly reflects MyoE powering, since similar tracks are not seen in *myoEΔ* kymographs. Irregular speeds might result from low myosin V processivity (Reck-Peterson *et al.*, 2001) and/or might be only apparent, reflecting the curling trajectories of actin cables in three dimensions (kymographs are plotted with 2D images). Small RabE^RAB11 carriers show uniform (2.5 μm/s on average) speeds, may reverse direction before they arrive to the apex, and follow regular and recurrent trajectories attributable to stiff MTs. The multiplicity of kinesins, the potential side effects of kinesin-null mutations on dynein (Zhang *et al.*, 2003) and MT stability (Requena *et al.*, 2001), and the likely MyoE assumption of kinesins' roles in the corresponding null mutants hindered the assignment of these trajectories to single kinesins.

RabE^RAB11 carriers bind actin cables without MyoE. Thus the F-actin tip "mop" actually "wipes" carriers. Potential candidates tethering carriers to actin might be nonmotile myosin domain–containing proteins, such as *U. maydis* Mcs1 (Schuster *et al.*, 2012), or even kinesin-1 itself (Hodges *et al.*, 2009). Actin depolymerization displaces exocytic RabE^RAB11 carriers to a kinesin/dynein-powered conveyor belt, an observation that we exploited to demonstrate that these carriers are loaded with MyoE, dynein, and one or more kinesins. RabE^RAB11, in concert with PsdIns4P, is the almost-certain MyoE recruiter, but the adaptors for kinesin and dynein are unknown. The presence of kinesins and MyoE on the same cargo might enhance each other's processivity (Ali *et al.*, 2008; Hodges *et al.*, 2009), as might tropomyosin in the tip actin cables enhance the processivity of MyoE during the final run (Hodges *et al.*, 2012).

A model of post-Golgi exocytic traffic: the conveyor belt relays carriers to actin cables

Post-Golgi structures (Figure 8, green ovals) originate anywhere within the cell by maturation of Golgi cisternae (red ovals and yellow ovals indicate cisternae before and during maturation,

respectively) and are loaded with motors as post-Golgi identity is acquired, thus becoming exocytic carriers. A carrier arising distally is transported by kinesin(s) to the tip, where the actin cable mop collects it. Then MyoE engages a cable and completes the delivery of the carrier to the apex. If myosin engagement fails, dynein drags the carrier away from the tip. Kinesins eventually counteract dynein, such that any carrier traveling basipetally may reverse direction to return to the tip, giving the carrier another chance to engage actin. Globally this results in MT-based bidirectional conveyor belt-like movement that becomes very conspicuous if F-actin is depolymerized. Given that the most apical Golgi equivalents are within reach of the actin cables (Figure 8), some RabE^RAB11 structures might be transported directly to the apex, and hence the relay mechanism may coexist with direct runs. MyoE is not essential because tip MTs are capable of delivering carriers directly to the plasma membrane. In the absence of MTs, those cisternae reached by actin cables maintain exocytosis with direct runs. This work also clarifies the evasive nature of the SPK. The vesicles that it contains are, at least in part, exocytic RabE^RAB11 carriers derived from the Golgi (Figure 8).

RAB11, hyphal cells, and melanocytes

The kinesin/myosin V relay mechanism operating in hyphal tips is conceptually similar to the "myosin V capture coupled to MT conveyor belt transport" proposed by Hammer and colleagues to explain the accumulation of melanosomes at the dendritic tips of melanocytes (Wu *et al.*, 1998). Indeed, our findings reveal that melanosome transport involving an exocytic organelle derived from the lysosome and the transport of exocytic post-Golgi carriers derived from Golgi cisternae evolved to use cooperation of cytoskeletal elements and their motors.

MATERIALS AND METHODS

Nomenclature

RabE^RAB11 and RabD^RAB8 are AN0347 and AN6974, respectively, in the AspGD database (www.aspgd.org).

Aspergillus strains, culture media, and genetic manipulation

A. nidulans standard growth media were used (Cove, 1966). For microscopy experiments, hyphae from strain MAD4120 or its derivatives (Supplemental Figure S2) were cultured in liquid "watch minimal medium" (Peñalva, 2005) containing 0.1% (wt/vol) glucose and 5 mM ammonium tartrate. In experiments involving strains carrying *alcA^P* -driven transgenes (indicated in the corresponding figure legends and described in what follows), we used 0.05–0.1% fructose (low expression levels) or 1% ethanol (high expression levels) instead of 1% glucose (which represses the promoter; Supplemental Figure S2). Strains carried markers in standard use. Strains are listed in Supplemental Table S1. Genetic crosses were performed with standard methods (Clutterbuck, 1993), and transformation was previously described (Tilburn *et al.*, 1983). The heterokaryon rescue technique for assessment of lethality associated with *rabEΔ* was used as described (Osmani *et al.*, 2006)

Gene expression constructs

These constructs are represented schematically in Supplemental Figure S2. For expressing GFP-RabE under the control of its natural promoter, we constructed by PCR fusion (Szewczyk et al., 2006) a $rabE^P::gfp-rabE::pyrG^{Af}::3'-UTR^{rabE}$ DNA molecule containing, from 5' to 3', the 5'-untranslated region (UTR) of $rabE$ amplified from genomic DNA with primers 7 and 8 (Supplemental Table S2); the $gfp-rabE$ transgene amplified from p1979 with primers 9 and 2; and a $pyrG^{Af}::3'UTR^{rabE}$ fragment previously generated by fusion PCR between the Aspergillus fumigatus $pyrG$ gene ($pyrG^{Af}$; amplified from p1530 (Osmani et al., 2006) with primers 10 and 11) with the 3'-UTR of $rabE$, amplified from genomic DNA with primers 12 and 13. The assembled molecule was cloned in pGEM t-easy to generate plasmid p2089, which was used to transform MAD1739. Southern blot analysis of transformants was used to select MAD4120, resulting from a single crossover event at the 3'-UTR of $rabE$. Thus this strain carries an in locus tandem duplication of $rabE$ with one of the copies tagged with GFP.

Plasmids p1979 and p2027 (plasmid numbers correspond to our −20°C collection of DNA molecules) drive expression of GFP- and mCherry-tagged $RabE^{RAB11}$, respectively, under the control of the $alcA^P$. These plasmids carry a nonfunctional mutant $argB*$ allele targeting integration to the $argB$ locus on chromosome III (Calcagno-Pizarelli et al., 2007). The $rabE$ open reading frame was amplified from a complete cDNA clone (p1815 in our plasmid collection) with primers 1 and 2 (Supplementary Table S2) and cloned into the BamHI/XhoI 6.92-kb fragment of p1398. Next coding regions of GFP (from p1929; Pantazopoulou and Peñalva, 2011; primers 3 and 4) or mCherry (from p1920; Abenza et al., 2012) were inserted into the BamHI site. The constructs were used to transform MAD540 (Supplemental Table S1). Single-copy integration events at $argB$ were identified by Southern blot (Supplemental Figure S2). Transformants MAD3069 and MAD3575 were used in subsequent genetic crosses. Using p1979 as template, we constructed a plasmid expressing mutant GDP-locked S23N-RabE (p2109), using Stratagene's site-directed mutagenesis kit with mutagenic primers 5 and 6 (Supplemental Table S2). MAD4271 carrying a single-copy integration of p2109 was selected after transformation of MAD1117.

To obtain $rabEΔ::pyrG^{Af}$ nuclei, the open reading frame of $rabE$ was substituted by the $pyrG^{Af}$ selection marker using a fragment obtained by fusion PCR (primers 15–20). The resulting linear $5'-UTR^{rabE}::pyrG^{Af}::3'-UTR^{rabE}$ molecule was transformed into $nkuAΔ::bar$ strain MAD1739, which carries $pyrG89$, resulting in pyrimidine auxotrophy. Viability could be rescued only in heterokaryosis with a $rabE^+$ allele. The $rabDΔ$ mutation was constructed by the same approach. $rabDΔ$ was recovered in homokaryosis (strain MAD3584 represents one of the multiple transformants obtained carrying the deletion allele, as determined by Southern blotting).

Plasmid p2090 drives expression of GFP-RabD under the control of the $alcA$ promoter. The plasmid carries a truncated, nonfunctional $pyroA*$ allele targeting integration to chromosome IV $pyroA4$ locus after selecting for pyridoxine auxotrophy (Calcagno-Pizarelli et al., 2007). For the construction of p2090, the GFP coding region was amplified from p1979 with primers 3 and 21 and cloned as a BamHI/EcoRI-digested fragment into p1920. Next the coding region of $rabD$ was amplified from a cDNA (p1783) clone with primers 22 and 23 and inserted as an EcoRI/XmaI fragment. p2090 was used to transform MAD1741. MAD4033 is a single-copy transformant.

Microscopy and quantitative analyses

We used a Leica DMI6000B inverted fluorescence microscope coupled to a Hamamatsu ORCA ERII camera with a Dual View beam splitter and the HCX 63×/1.4 numerical aperture objective. The microscope was driven by MetaMorph (Molecular Devices). Microscopy was in all cases made in vivo, using Lab-Tek chambers (Nalge Nunc International, Rochester, NY). Culture temperature control, other aspects of the microscopy setup, and the methodology for the "on-stage" temperature shift experiments have been described in detail (Pinar et al., 2013a). For the quantitation of the GFP-RabE^{RAB11} signal at the SPK we used sum projections derived from Z-stacks of images acquired under the same conditions to calculate the overall signal in equivalent circular regions of interest. BFA, benomyl, and latB were used at 200, 5–10, and 40 μg/ml, respectively.

For multidimensional sequences (x, y, z, four to six planes every 0.35 μm; t, 3- to 4-s intervals; w, two channels acquired simultaneously with a Dual View beam splitter) were deconvolved with the CMLE algorithm of Huygens Professional (www.svi.nl). Maximal-intensity projections of the two channels were aligned with MetaMorph and used to measure the integrated fluorescence intensity of a circular region containing a cisterna, whose position was manually adjusted for each time point to correct short-range movement. Measurements were carried out in time sequences that covered the complete maturation cycle. These values were normalized and plotted against time. Graphs corresponding to different maturation events were aligned relative to the time points showing the maximum mRFP-PH^{OSBP} or HypB^{Sec7}-GFP channel value, which was set as 100%. For measuring the lifetime of PH^{OSBP} (Figure 2) or HypB^{Sec7} (Supplemental Figure S3) LGC, we considered the time between the earliest detection of an increase in mRFP-PH^{OSBP} fluorescence and the time at which fluorescence dropped to near background. For RabE, we determined the "residence time" associated with a LGC as the period between the frame at which GFP-RabE was first detected in an mRFP-PH^{OSBP} LGC and the time at which the RabE-enriched membranes underwent movement. All measurements were made in hyphae maintaining apical extension.

FRAP experiments used a Leica SP5 confocal microscope and a 488-nm argon laser, using the Leica LAS FRAP wizard. Photobleaching (five cycles) with 60% of the laser power bleached the SPK GFP-RabE signal in middle hyphal tip planes to background levels. From 5 to 10 prebleaching and from 50 to 90 postbleaching frames were acquired every 2 s (4% laser power). These conditions were compatible with hyphal growth (thus with exocytosis). The integrated intensity values of the region of interest were background subtracted and normalized, setting the maximal prebleach value as 100%. Curve fitting used Prism, version 6 (GraphPad), using the one-phase association equation to calculate recovery $t_{1/2}$.

REFERENCES

Abenza JF, Galindo A, Pantazopoulou A, Gil C, de los Ríos V, Peñalva MA (2010). *Aspergillus* RabB^Rab5 integrates acquisition of degradative identity with the long-distance movement of early endosomes. Mol Biol Cell 21, 2756–2769.

Abenza JF, Galindo A, Pinar M, Pantazopoulou A, de los Ríos V, Peñalva MA (2012). Endosomal maturation by Rab conversion in *Aspergillus nidulans* is coupled to dynein-mediated basipetal movement. Mol Biol Cell 23, 1889–1901.

Abenza JF, Pantazopoulou A, Rodríguez JM, Galindo A, Peñalva MA (2009). Long-distance movement of *Aspergillus nidulans* early endosomes on microtubule tracks. Traffic 10, 57–75.

Ali MY, Lu H, Bookwalter CS, Warshaw DM, Trybus KM (2008). Myosin V and Kinesin act as tethers to enhance each others' processivity. Proc Natl Acad Sci USA 105, 4691–4696.

Barr FA (2013). Review series: Rab GTPases and membrane identity: causal or inconsequential? J Cell Biol 202, 191–199.

Behnia R, Munro S (2005). Organelle identity and the signposts for membrane traffic. Nature 438, 597–604.

Bonifacino JS, Glick BS (2004). The mechanisms of vesicle budding and fusion. Cell 116, 153–166.

Cabrera M, Ungermann C (2013). Guanine nucleotide exchange factors (GEFs) have a critical but not exclusive role in organelle localization of Rab GTPases. J Biol Chem 288, 28704–28712.

Calcagno-Pizarelli AM *et al.* (2007). Establishment of the ambient pH signaling complex in *Aspergillus nidulans*: PalI assists plasma membrane localization of PalH. Eukaryot Cell 6, 2365–2375.

Chen SH, Chen S, Tokarev AA, Liu F, Jedd G, Segev N (2005). Ypt31/32 GTPases and their novel F-box effector protein Rcy1 regulate protein recycling. Mol Biol Cell 16, 178–192.

Chen SH, Shah AH, Segev N (2011). Ypt31/32 GTPases and their F-Box effector Rcy1 regulate ubiquitination of recycling proteins. Cell Logist 1, 21–31.

Clutterbuck AJ (1993). *Aspergillus nidulans*. In: Genetic Maps, Vol. 3: Locus Maps of Complex Genomes, 6th ed., SJ O'Brien, Cold Spring Harbor, NY: Cold Spring Harbor Laboratory Press, 3.71–3.84.

Cove DJ (1966). The induction and repression of nitrate reductase in the fungus *Aspergillus nidulans*. Biochim Biophys Acta 113, 51–56.

Daboussi L, Costaguta G, Payne GS (2012). Phosphoinositide-mediated clathrin adaptor progression at the *trans*-Golgi network. Nat Cell Biol 14, 239–248.

Donovan KW, Bretscher A (2012). Myosin-V is activated by binding secretory cargo and released in coordination with Rab/exocyst function. Dev Cell 23, 769–781.

Glick BS, Luini A (2011). Models for Golgi traffic: a critical assessment. Cold Spring Harb Perspect Biol 3, a005215.

Glick BS, Nakano A (2009). Membrane traffic within the Golgi apparatus. Annu Rev Cell Dev Biol 25, 113–132.

Harris SD, Read ND, Roberson RW, Shaw B, Seiler S, Plamann M, Momany M (2005). Polarisome meets Spitzenkörper: microscopy, genetics, and genomics converge. Eukaryot Cell 4, 225–229.

Hodges AR, Bookwalter CS, Krementsova EB, Trybus KM (2009). A nonprocessive class V myosin drives cargo processively when a kinesin-related protein is a passenger. Curr Biol 19, 2121–2125.

Hodges AR, Krementsova EB, Bookwalter CS, Fagnant PM, Sladewski TE, Trybus KM (2012). Tropomyosin is essential for processive movement of a class V myosin from budding yeast. Curr Biol 22, 1410–1416.

Hohmann-Marriott MF, Uchida M, van de Meene AM, Garret M, Hjelm BE, Kokoori S, Roberson RW (2006). Application of electron tomography to fungal ultrastructure studies. New Phytol 172, 208–220.

Horio T, Oakley BR (2005). The role of microtubules in rapid hyphal tip growth of *Aspergillus nidulans*. Mol Biol Cell 16, 918–926.

Jedd G, Mulholland J, Segev N (1997). Two new Ypt GTPases are required for exit from the yeast trans-Golgi compartment. J Cell Biol 137, 563–580.

Jin Y, Sultana A, Gandhi P, Franklin E, Hamamoto S, Khan AR, Munson M, Schekman R, Weisman LS (2011). Myosin V transports secretory vesicles via a Rab GTPase cascade and interaction with the exocyst complex. Dev Cell 21, 1156–1170.

Konzack S, Rischitor PE, Enke C, Fischer R (2005). The role of the kinesin motor KipA in microtubule organization and polarized growth of *Aspergillus nidulans*. Mol Biol Cell 16, 497–506.

Lenz JH, Schuchardt I, Straube A, Steinberg G (2006). A dynein loading zone for retrograde endosome motility at microtubule plus-ends. EMBO J 25, 2275–2286.

Levine TP, Munro S (2002). Targeting of Golgi-specific pleckstrin homology domains involves both PtdIns 4-kinase-dependent and -independent components. Curr Biol 12, 695–704.

Lipatova Z, Tokarev AA, Jin Y, Mulholland J, Weisman LS, Segev N (2008). Direct interaction between a myosin V motor and the Rab GTPases Ypt31/32 is required for polarized secretion. Mol Biol Cell 19, 4177–4187.

Losev E, Reinke CA, Jellen J, Strongin DE, Bevis BJ, Glick BS (2006). Golgi maturation visualized in living yeast. Nature 441, 1002–1006.

Matsuura-Tokita K, Takeuchi M, Ichihara A, Mikuriya K, Nakano A (2006). Live imaging of yeast Golgi cisternal maturation. Nature 441, 1007–1010.

Mizuno-Yamasaki E, Medkova M, Coleman J, Novick P (2010). Phosphatidylinositol 4-phosphate controls both membrane recruitment and a regulatory switch of the Rab GEF Sec2p. Dev Cell 18, 828–840.

Morozova N, Liang Y, Tokarev AA, Chen SH, Cox R, Andrejic J, Lipatova Z, Sciorra VA, Emr SD, Segev N (2006). TRAPPII subunits are required for the specificity switch of a Ypt-Rab GEF. Nat Cell Biol 8, 1263–1269.

Nordmann M, Cabrera M, Perz A, Brocker C, Ostrowicz C, Engelbrecht-Vandre S, Ungermann C (2010). The Mon1-Ccz1 complex is the GEF of the late endosomal Rab7 homolog Ypt7. Curr Biol 20, 1654–1659.

Novick P, Field C, Schekman R (1980). Identification of 23 complementation groups required for post-translational events in the yeast secretory pathway. Cell 21, 205–215.

Ortiz D, Medkova M, Walch-Solimena C, Novick P (2002). Ypt32 recruits the Sec4p guanine nucleotide exchange factor, Sec2p, to secretory vesicles; evidence for a Rab cascade in yeast. J Cell Biol 157, 1005–1015.

Osmani AH, Oakley BR, Osmani SA (2006). Identification and analysis of essential *Aspergillus nidulans* genes using the heterokaryon rescue technique. Nat Protoc 1, 2517–2526.

Pantazopoulou A, Peñalva MA (2009). Organization and dynamics of the *Aspergillus nidulans* Golgi during apical extension and mitosis. Mol Biol Cell 20, 4335–4347.

Pantazopoulou A, Peñalva MA (2011). Characterization of *Aspergillus nidulans* RabC^Rab6. Traffic 12, 386–406.

Patterson GH, Hirschberg K, Polishchuk RS, Gerlich D, Phair RD, Lippincott-Schwartz J (2008). Transport through the Golgi apparatus by rapid partitioning within a two-phase membrane system. Cell 133, 1055–1067.

Pearson CL, Xu K, Sharpless KE, Harris SD (2004). MesA, a novel fungal protein required for the stabilization of polarity axes in *Aspergillus nidulans*. Mol Biol Cell 15, 3658–3672.

Peñalva MA (2005). Tracing the endocytic pathway of *Aspergillus nidulans* with FM4-64. Fungal Genet Biol 42, 963–975.

Peñalva MA, Galindo A, Abenza JF, Pinar M, Calcagno-Pizarelli AM, Arst HNJr, Pantazopoulou A (2012). Searching for gold beyond mitosis: mining intracellular membrane traffic in *Aspergillus nidulans*. Cell Logist 2, 2–14.

Peplowska K, Markgraf DF, Ostrowicz CW, Bange G, Ungermann C (2007). The CORVET tethering complex interacts with the yeast Rab5 homolog Vps21 and is involved in endo-lysosomal biogenesis. Dev Cell 12, 739–750.

Pinar M, Pantazopoulou A, Arst HN Jr, Peñalva MA (2013a). Acute inactivation of the *Aspergillus nidulans* Golgi membrane fusion machinery: correlation of apical extension arrest and tip swelling with cisternal disorganization. Mol Microbiol 89, 228–248.

Pinar M, Pantazopoulou A, Peñalva MA (2013b). Live-cell imaging of *Aspergillus nidulans* autophagy: RAB1 dependence, Golgi independence and ER involvement. Autophagy 9, 1–20.

Reck-Peterson SL, Tyska MJ, Novick PJ, Mooseker MS (2001). The yeast class V myosins, Myo2p and Myo4p, are nonprocessive actin-based motors. J Cell Biol 153, 1121–1126.

Requena N, Alberti-Segui C, Winzenburg E, Horn C, Schliwa M, Philippsen P, Liese R, Fischer R (2001). Genetic evidence for a microtubule-destabilizing effect of conventional kinesin and analysis of its consequences for the control of nuclear distribution in *Aspergillus nidulans*. Mol Microbiol 42, 121–132.

Rivera-Molina FE, Novick PJ (2009). A Rab GAP cascade defines the boundary between two Rab GTPases on the secretory pathway. Proc Natl Acad Sci USA 106, 14408–14413.

Santiago-Tirado FH, Legesse-Miller A, Schott D, Bretscher A (2011). PI4P and Rab inputs collaborate in myosin-V-dependent transport of secretory compartments in yeast. Dev Cell 20, 47–59.

Schuster M, Lipowsky R, Assmann MA, Lenz P, Steinberg G (2011). Transient binding of dynein controls bidirectional long-range motility of early endosomes. Proc Natl Acad Sci USA 108, 3618–3623.

Schuster M, Treitschke S, Kilaru S, Molloy J, Harmer NJ, Steinberg G (2012). Myosin-5, kinesin-1 and myosin-17 cooperate in secretion of fungal chitin synthase. EMBO J 31, 214–227.

Sclafani A, Chen S, Rivera-Molina F, Reinisch K, Novick P, Ferro-Novick S (2010). Establishing a role for the GTPase Ypt1p at the late Golgi. Traffic 11, 520–532.

Sharpless KE, Harris SD (2002). Functional characterization and localization of the *Aspergillus nidulans* formin SEPA. Mol Biol Cell 13, 469–479.

Suda Y, Kurokawa K, Hirata R, Nakano A (2013). Rab GAP cascade regulates dynamics of Ypt6 in the Golgi traffic. Proc Natl Acad Sci USA 110, 18976–18981.

Szewczyk E, Nayak T, Oakley CE, Edgerton H, Xiong Y, Taheri-Talesh N, Osmani SA, Oakley BR (2006). Fusion PCR and gene targeting in *Aspergillus nidulans*. Nat Protoc 1, 3111–3120.

Taheri-Talesh N, Horio T, Araujo-Bazán LD, X, Espeso EA, Peñalva MA, Osmani SA, Oakley BR (2008). The tip growth apparatus of *Aspergillus nidulans*. Mol Biol Cell 19, 1439–1449.

Taheri-Talesh N, Xiong Y, Oakley BR (2012). The functions of myosin II and myosin V homologs in tip growth and septation in *Aspergillus nidulans*. PLoS One 7, e31218.

Tilburn J, Scazzocchio C, Taylor GG, Zabicky-Zissman JH, Lockington RA, Davies RW (1983). Transformation by integration in *Aspergillus nidulans*. Gene 26, 205–211.

Torralba S, Raudaskoski M, Pedregosa AM, Laborda F (1998). Effect of cytochalasin A on apical growth, actin cytoskeleton organization and enzyme secretion in *Aspergillus nidulans*. Microbiology 144, 45–53.

Virag A, Lee MP, Si H, Harris SD (2007). Regulation of hyphal morphogenesis by *cdc42* and *rac1* homologues in *Aspergillus nidulans*. Mol Microbiol 66, 1579–1596.

Wooding S, Pelham HRB (1998). The dynamics of Golgi protein traffic visualized in living yeast cells. Mol Biol Cell 9, 2667–2680.

Wu X, Bowers B, Rao K, Wei Q, Hammer JA 3rd (1998). Visualization of melanosome dynamics within wild-type and dilute melanocytes suggests a paradigm for myosin V function in vivo. J Cell Biol 143, 1899–1918.

Yang Y, El Ganiny AM, Bray GE, Sanders DAR, Kaminskyj SGW (2008). *Aspergillus nidulans hypB* encodes a Sec7-domain protein important for hyphal morphogenesis. Fungal Genet Biol 45, 749–759.

Zhang J, Li S, Fischer R, Xiang X (2003). Accumulation of cytoplasmic dynein and dynactin at microtubule plus ends in *Aspergillus nidulans* is kinesin dependent. Mol Biol Cell 14, 1479–1488.

Zhang J, Tan K, Wu X, Chen G, Sun J, Reck-Peterson SL, Hammer JA 3rd, Xiang X (2011). *Aspergillus* myosin-V supports polarized growth in the absence of microtubule-based transport. PLoS One 6, e28575.